Journal of Catalysis **211,** 216–225 (2002)
doi:10.1006/jcat.2002.3732

Effects of Metal Cation on the Skeletal Isomerization of 1-Butene over Clinoptilolite

Hyun Chul Lee,* Hee Chul Woo,† Soo Hyun Chung,‡ Hae Jin Kim,§ Kyung Hee Lee,* and Jae Sung Lee*,[1]

*Department of Chemical Engineering, Pohang University of Science and Technology (POSTECH), Pohang 790-784, South Korea; †Department of Chemical Engineering, Pukyong National University, Pusan 608-739, South Korea; ‡Korea Institute of Energy Research, Daejeon 305-343, South Korea; and §Department of Chemistry and Division of Molecular and Life Science, Pohang University of Science and Technology (POSTECH), Pohang 790-784, South Korea

Received March 19, 2002; revised June 11, 2002; accepted June 27, 2002

Skeletal isomerization of 1-butene to isobutene has been investigated over various metal-cation-exchanged natural clinoptilolite zeolites. The effects of metal cation exchange were examined by XRD, NH_3-TPD, FT-IR, and solid-state NMR to elucidate the controlling factors affecting the selectivity to isobutene. Cobalt-cation-exchanged natural clinoptilolite zeolite (Co–HNZ) showed a higher selectivity to isobutene compared with that of HNZ at the same conversion of *n*-butenes under the same reaction conditions, while barium-cation-exchanged zeolite (Ba–HNZ) exhibited a higher activity but a very low selectivity to isobutene. It could be suggested that the high selectivity over the Co–HNZ catalyst was induced by selective removal of strong acid sites that were responsible for the side reactions of dimerization cracking as well as by imposing an effective constraint on zeolite channels. On the other hand, the high density and easy accessibility of acid sites mainly on the external surface in Ba–HNZ could increase the extent of the bimolecular reaction pathway, leading to high yields of by-products. Thus, a selective catalyst for skeletal isomerization of 1-butene should satisfy multiple requirements regarding its acid site, namely, strength, type, concentration, and accessibility.

Key Words: **clinoptilolite; skeletal isomerization; acidity; selectivity; cobalt; FT-IR; NMR.**

INTRODUCTION

Isobutene is an important raw material for the synthesis of many chemicals and polymers, including methyl-tertiary-butyl ether (1), methyl methacrylate, butyl rubber, and polybutene. A promising route to produce isobutene independently is the catalytic skeletal isomerization of linear butenes to isobutene. The status of the technology has been summarized in recent reviews (2, 3).

The most efficient catalysts for the skeletal isomerization of *n*-butenes to isobutene are known to be zeolites and molecular sieves such as ferrierite (4–6), ZSM-22 (7), ZSM-23 (8), and Me-APO-11 (9). The salient features of these effective catalysts for skeletal isomerization of *n*-butenes are unique pore structure with a 10-membered ring and proper strength and density of the acid sites (10–12). Houžvička *et al.* (11) reported the effects of zeolite pore structure on skeletal isomerization of *n*-butenes. The authors have shown that the most suitable structures are 10-membered-ring zeolites with the pore diameter of 4.0–5.5 Å, while 8- and 12-membered-ring zeolites are not suitable materials, due to excessively restricted diffusion of isobutene for the 8-membered rings and inability to suppress effectively the formation of carbonaceous deposits for the 12-membered rings.

Factors affecting the selectivity of isobutene in the skeletal isomerization of 1-butene include distribution, types and character of the acid sites, and shape-selective effect. Seo *et al.* (13, 14) have suggested that the higher selectivity of isobutene is obtained by isolation of each activated butene molecule on the catalyst surface, leading to suppression of undesired by-product formation by dimerization followed by cracking of dimers. Thus, the low density of acid sites becomes important for high isomerization selectivity.

Clinoptilolite, used in this study as a catalyst, is one of the most abundant zeolites in nature. It is a silica-rich member of the heulandite family (15). It has a pore structure of a monoclinic framework with a two-dimensional channel system consisting of 10-membered-ring (7.5 × 3.1 Å) channels and 8-membered-ring (3.6 × 4.6 Å) channels viewed along [001], which are intersected by 8-membered-ring (4.7 × 2.8 Å) channels viewed along [100]. Applications of clinoptilolite as catalysts have been reported in many previous works (16–19). We already confirmed that clinoptilolite zeolites were an effective catalyst for skeletal isomerization of *n*-butenes to isobutene (20, 21).

In this study, we modified the natural clinoptilolite zeolite by introducing various metal cations and investigated its effect on the nature of acid sites (Brønsted vs Lewis acid sites), which, in turn, should affect the conversion of *n*-butenes and the selectivity into isobutene in the skeletal

[1] To whom correspondence should be addressed. Fax: (+82-54) 279-5528. E-mail: jlee@postech.ac.kr.

0021-9517/02 $35.00

isomerization of 1-butene. The strength, type, and density of these acid sites were changed according to the introduced metal cations. These acid characteristics of modified natural clinoptilolites were investigated by means of NH_3-TPD, FT-IR, and solid-state NMR.

EXPERIMENTAL

Preparation of Catalysts

Natural zeolite, clinoptilolite, employed as a catalyst in this study, was obtained from the Youngil area of South Korea. The natural zeolite (NZ) was ion exchanged four times with 1 M NH_4Cl solution at 353 K for 24 h. The obtained ammonium form of the natural zeolite (NH_4^+–NZ) was filtered with hot distilled water and dried at 383 K for 16 h. Finally, the proton-form natural zeolite (HNZ) having strong acid sites was prepared by calcining NH_4^+–NZ at 773 K for 4 h under flow of air.

In order to modify the acid characteristics of the proton-form natural zeolite, HNZ was ion exchanged again with aqueous solutions of alkaline earth metals, Ni, Mn, Cu, and Co. In all cases, the ion exchange was carried out with a 0.01 M nitrate solution (100 ml per g of the zeolite) at 368 K for 20 h under reflux condition. The HNZ was also impregnated with metal cations by the incipient wetness method to compare preparation methods. After ion exchange with a metal cation, the resulting modified catalysts were dried and calcined at 773 K for 4 h. The cobalt loading for Co–HNZ ion exchanged with 0.01 M solution was found to be 0.87 wt%. We also compared catalytic performance of HNZ and metal-ion-exchanged HNZ with that of ferrierite (FER), known as one of the most efficient catalysts for the skeletal isomerization of 1-butene, which was synthesized according to the procedure reported in the literature (22).

Characterization of Catalysts

To examine the crystallinity of the prepared catalysts, XRD (MAC Science Co, M18XHF) analysis with Cu $K\alpha$ radiation was carried out. The Si/Al ratio and the amount of metal loaded to HNZ were determined by induced coupled plasma (ICP) analysis. The surface area and micropore volume was determined from nitrogen adsorption and desorption isotherm data obtained on a constant-volume adsorption apparatus (Micromeritics ASAP 2010).

In order to examine the acidity of natural zeolites modified by the metal ion exchange, NH_3-TPD experiments were performed on a flow reaction system. A sample of 30 mg was preheated from room temperature (RT) to 773 K under a helium flow of 59.5 μmol/s at a ramping rate of 10 K/min. After cooling to 373 K, then NH_3 was adsorbed by flowing NH_3 onto the sample for 0.5 h. After purging the system to remove physisorbed species by He flow for 1 h, the sample was heated from 373 to 1123 K at a ramping rate of 10 K/min. The desorbed NH_3 was monitored by a mass spectrometer (HP5972 MSD).

To identify the types of the acid sites in HNZ, metal-ion-exchanged HNZs, and ferrierite, FT-IR spectra were recorded on a Perkin–Elmer 1800 Fourier transform infrared spectrophotometer with a resolution of 2 cm^{-1} for the samples made into self-supporting wafers. The self-supporting wafers (10 mg) were evacuated at 773 K for 1 h in an *in situ* IR cell equipped with CaF_2 windows. The FT-IR spectra for the hydroxyl group of zeolites were recorded in the region of 3800–3000 cm^{-1}. For the identification of the types of the acid site (Brønsted and Lewis acid sites), pyridine was adsorbed at 473 K for 0.5 h and the IR cell was evacuated to eliminate physisorbed species at 523 K for 2 h. The spectra of pyridine chemisorbed on zeolites were obtained in the region of 1600–1400 cm^{-1}.

Solid-state NMR measurements to investigate the structural change were performed on a Varian Unity *Inova* 300 MHz spectrometer equipped with a 7-mm Chemagnetics MAS probe head using a sample rotation rate of 6 kHz. The spectra of ^{27}Al MAS, CP MAS, and ^{29}Si MAS were measured at frequencies of 78.156 and 59.590 MHz. Chemical shifts were measured in parts per million with respect to $Al(H_2O)_6^{3+}$ and tetramethylsilane(TMS) as references for ^{27}Al and ^{29}Si, respectively.

The amount of coke deposited after reaction was measured on a CHNS analyzer (LECO Co, CHNS-932) and also compared with TPO (temperature-programmed oxidation) experiments in which the used catalyst was heated from room temperature to 1173 K at a ramping rate of 10 K/min using a 1% O_2/He flow. The desorbed CO_2 was monitored by a mass spectrometer (HP5972 MSD).

Catalytic Reactions

Skeletal isomerization reactions were carried out in a continuous fixed-bed reactor under atmospheric pressure. The sample was preheated at 773 K for 1 h under H_2 flow. After cooling the temperature to the desired temperature, the reactant stream of 1-butene (Matheson) was fed to the reactor at a rate of 3.7 μmol/s. The total flow rate including H_2 as a diluent gas was maintained at 18.6 μmol/s. The products of reaction were analyzed by an online gas chromatograph with a Hewlett–Packard 5890 series II equipped with a column of 20% BMEA (24 ft long, from Craw) and a flame ionization detector. Since rapid equilibrium of double-bond isomerization was established under the condition of the present study, 2-butenes could also be transformed to isobutene, and thus all linear butenes were regarded as reactants. Thus, the conversion was calculated from the consumed *n*-butenes and the selectivity to isobutene from moles of produced isobutene divided by moles of consumed *n*-butenes.

TABLE 1

Comparison of Catalytic Activity over HNZ and Other Various Metal-Cation-Containing HNZs at 5 h Time on Stream

Method	Catalysts	Conversion (%)	Selectivity (%)				Yield (%)
			$C_3 + C_5$	*n*-Butane	Isobutane	Isobutene	
	HNZ	38.78	14.92	2.22	1.53	78.51	30.44
Incipient wetness	Co (1 wt%)	26.46	6.039	5.97	0.77	83.33	22.05
	Ni (1 wt%)	31.43	12.27	2.28	1.52	78.41	24.64
	Zn (1 wt%)	28.04	14.77	1.88	2.00	76.28	21.39
Ion exchange	Co (0.01 M)	38.90	9.85	1.87	1.13	82.75	32.19
	Mg (0.01 M)	22.95	22.08	3.99	1.99	67.53	15.50
	Ca (0.01 M)	36.67	23.34	2.38	2.60	76.18	27.94
	Sr (0.01 M)	40.87	29.08	14.89	3.13	56.97	23.28
	Ba (0.01 M)	45.55	23.41	4.22	2.76	65.17	29.68
	Ni (0.01 M)	32.62	12.30	2.53	1.59	75.78	24.72
	Zn (0.01 M)	23.53	17.63	3.05	2.27	65.24	15.35
	Mn (0.01 M)	34.25	28.24	10.43	3.18	62.34	21.35
	Cu (0.01 M)	35.32	16.93	2.62	2.16	73.67	26.02
	Co (0.03 M)	28.19	10.85	2.19	1.15	80.04	22.57

Note. Reaction conditions: $T = 723$ K, WHSV $= 1.5$ h^{-1}, $H_2/C_4 = 4$, atmospheric pressure.

RESULTS

Catalytic Performance of Metal-Cation-Exchanged HNZ

Various metal cations were exchanged with the proton form of natural clinoptilolite zeolite (HNZ) in order to investigate the effect of metal cation on the skeletal isomerization of 1-butene to isobutene. Table 1 exhibits the comparative catalytic performance of metal-cation-exchanged clinoptilolite zeolites. Among the modified zeolites, those containing cobalt ion were unique in showing higher selectivity of isobutene, the desired product in the skeletal isomerization of 1-butene, compared to unmodified HNZ, regardless of the method of preparation and the amount of cobalt loading. However, a marked decrease in conversion of *n*-butenes was observed for the modified catalyst prepared by incipient impregnation or by ion exchange with a high concentration of cobalt ion (0.03 M). Other modified zeolites with various metal cations showed relatively low selectivities of isobutene. An interesting feature of alkaline earth metal-ion-exchanged zeolites was that the conversion of *n*-butenes increased progressively as one went from Mg^{2+}- to Ba^{2+}-cation-exchanged zeolites. These catalysts, however, showed low selectivities to isobutene, mainly due to the enhanced formation of by-products ($C_3 + C_5$) via dimerization followed by cracking reaction.

The change with time on stream is compared in Fig. 1 for catalytic performance of clinoptilolite zeolite (HNZ), metal-cation-exchanged zeolites (Co–HNZ and Ba–HNZ), and ferrierite in the skeletal isomerization of 1-butene to isobutene. The Co–HNZ showed higher selectivity to isobutene than those of the other catalysts for all time on stream under the present reaction conditions: $T = 723$ K, $H_2/C_4 = 4$, WHSV $= 1.5$ h^{-1}. Moreover, Co–HNZ exhibited little difference in the conversion of *n*-butenes compared with that of the unmodified zeolite. In the case of Ba–HNZ, a selectivity higher than that of HNZ was observed

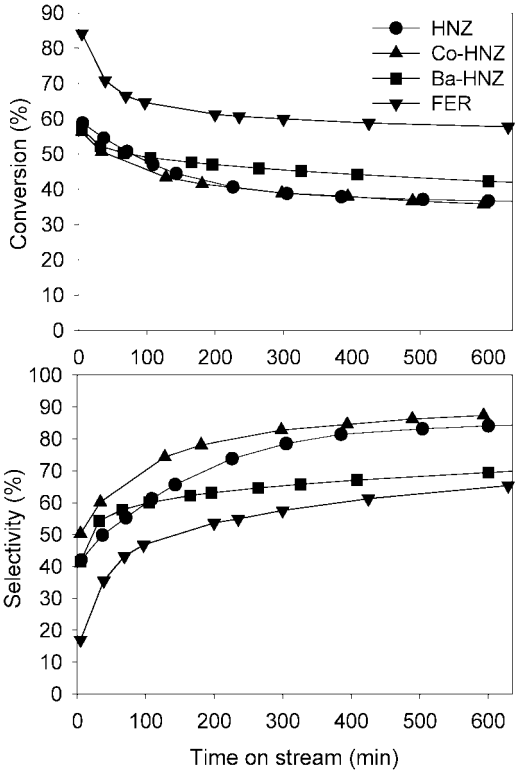

FIG. 1. The skeletal isomerization of 1-butene to isobutene over HNZ, Co–HNZ, Ba–HNZ, and ferrierite. Reaction conditions; $T = 723$ K, WHSV $= 1.5$ h^{-1}, $H_2/C_4 = 4$, atmospheric pressure.

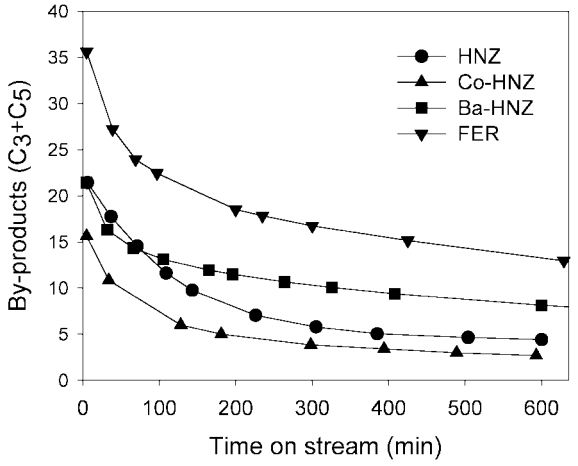

FIG. 2. Comparison of by-products ($C_3 + C_5$) over HNZ, Co–HNZ, Ba–HNZ, and ferrierite under the reaction conditions of $T = 723$ K, WHSV $= 1.5$ h^{-1}, $H_2/C_4 = 4$, atmospheric pressure.

only briefly in the early stage of the reaction and then the trend was reversed with time on stream. The Ba–HNZ revealed higher and more stable conversions with time on stream than those of HNZ and Co–HNZ. Unfortunately, the catalyst also showed the highest by-products ($C_3 + C_5$) formation for the whole time on stream, as shown in Fig. 2. Ferrierite, known as the most effective catalyst for this reaction, showed higher conversions but lower selectivities than those of HNZ-derived catalysts forming large amounts of by-products ($C_3 + C_5$). Isobutene selectivity in Fig. 1 and by-products formation in Fig. 2 show opposite trends with time, indicating that the formation of ($C_3 + C_5$) products is the main reason for the reduced selectivity.

Product distributions of skeletal isomerization of 1-butene at a time on stream of 200 min are shown in Table 2. The high selectivity of Co–HNZ could be attributed to the suppression of the dimerization of *n*-butenes, the main competitive side reaction leading to formation of by-products ($C_3 + C_5$) by subsequent cracking. On the other hand, Ba–HNZ and ferrierite produced higher amounts of by-products, leading to low selectivities to isobutene. The excessive amount of by-products for ferrierite resulted in the fairly low selectivity. All the clinoptilolite zeolites showed higher selectivities than that of ferrierite under the same reaction conditions. The difference in selectivity of isobutene between ferrierite and clinoptilolite zeolites has been attributed to different pore sizes and shapes (23). Although both zeolites have both 10- and 8-membered rings in their pore structure, clinoptilolite zeolite has more restricted spatial constraints in its pores (15).

The amount of coke deposited after the reaction was investigated by TPO experiments under the flow of 1% O_2 balanced with He. Figure 3 represents the profiles of TPO

TABLE 2

Product Distribution of Skeletal Isomerization of 1-Butene to Isobutene at 200 min Time on Stream over HNZ, Modified HNZs, and FER

Products	HNZ	Co–HNZ	Ba–HNZ	FER
C_1	0.72	0.91	0.83	0.54
C_2	1.35	1.85	1.88	2.12
C_3	4.92	3.05	7.62	12.42
Isobutane	0.72	0.50	1.39	3.03
n-Butane	1.28	0.92	1.97	2.81
1-Butene	10.42	10.01	9.81	5.94
Isobutene	29.74	32.27	29.59	32.78
Trans-2-butene	27.35	27.85	24.50	18.35
Cis-2-butene	20.66	20.99	18.56	14.40
1,3-Butadiene	0	0	0	1.54
Heavier (C_{5+})	2.84	1.65	3.85	6.07
Trans/*Cis*	1.32	1.33	1.32	1.27
Conversion (%)	41.46	41.04	47.03	61.24
Selectivity (%)	71.87	78.78	63.04	53.63
Yield (%)	29.80	32.33	29.65	32.84

Note. Reaction conditions: $T = 723$ K, WHSV $= 1.5$ h^{-1}, $H_2/C_4 = 4$, atmospheric pressure.

for used HNZ and Co–HNZ after 10 h of the reaction. The amount of desorbed CO_2 for Co–HNZ was less than that of HNZ. Furthermore, the maximum peak temperature of desorbed CO_2 was shifted toward a lower temperature for Co–HNZ. The amounts of coke measured by the CHNO analyzer after 10 h of the reaction were 5.25 and 3.98 wt% for HNZ and Co–HNZ, respectively. As discussed previously elsewhere (20), this coke deactivates the zeolite catalysts by blocking the pores, but it improves the isobutene selectivity by modifying zeolite pore structure, particularly in the early stage of the reaction.

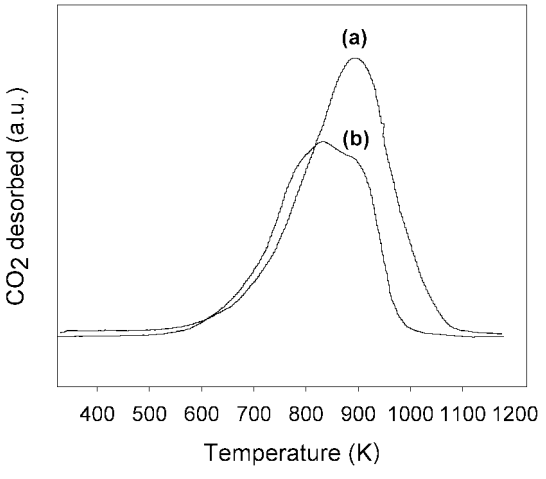

FIG. 3. TPO (temperature-programmed oxidation) profile of HNZ and Co–HNZ under the flow of 1% O_2 balanced with He. (a) HNZ, (b) Co–HNZ.

TABLE 3

Physicochemical Properties of HNZ, Co–HNZ, Ba–HNZ, and Ferrierite

Catalyst	Si/Al ratio (ICP analysis/NMR)	BET surface area (m^2/g)	Micropore volume[a] (cm^3/g)	Selectivity (%)	Yield[b] (%)
HNZ	4.4/4.1	219.3	0.076	71.87	29.80
Co–HNZ[c]	3.6/5.0	161.8	0.051	78.78	32.33
Ba–HNZ[d]	4.8/4.0	94.1	0.027	63.04	29.65
Ferrierite	16.2/—	210.7	0.083	53.63	32.84

[a] Calculated by the *t*-plot method.

[b] Yield of isobutene after 200 min of the reaction at 723 K (WHSV = 1.5 h^{-1}, $H_2/C_4 = 4$).

[c] HNZ ion exchanged with 0.01 M aqueous solution of $Co(NO_3)_26H_2O$ at 368 K for 20 h containing 0.87 wt% Co.

[d] HNZ ion exchanged with 0.01 M aqueous solution of $Ba(NO_3)_2$ at 368 K for 20 h containing 5.46 wt% Ba.

Characterization of Metal-Cation-Exchanged HNZ

Among natural zeolites modified with various metal cations (denoted Me–HNZ), Co–HNZ showed an improved catalytic performance in the skeletal isomerization of 1-butene to isobutene, by showing a higher selectivity to isobutene compared with that of HNZ and the other Me–HNZs. This is more significant because the improvement in selectivity was achieved without any sacrifice in *n*-butene conversion. Improvement in conversion over Ba–HNZ is also interesting although it accompanies the decrease in isobutene selectivity. Hence, these catalysts were characterized in more detail and compared with ferrierite, a better-studied catalyst for the reaction. Table 3 shows physicochemical properties of HNZ, metal-cation-exchanged HNZs (Co–HNZ and Ba–HNZ), and ferrierite. BET surface areas and micropore volumes of metal-cation-exchanged HNZs were reduced from those of HNZ. For the case of Ba–HNZ, the loss was larger than those of Co–HNZ, probably due to partial collapse of the framework during ion exchange of the bulky barium cation, as evidenced by the reduced XRD intensity in Fig. 4e.

Figure 4 shows the XRD patterns of metal-cation-exchanged HNZs. Though a slight decrease in intensity of the main peaks was observed, modified catalysts maintained their framework structure during ion exchange and subsequent steps. Especially, Ba–HNZ showed lower crystallinity than that of Co–HNZ due to partial destruction of framework, but it still retained clinoptilolite structure. In addition, it appeared that the introduction of metal cations by exchange with proton in HNZ would lead to partial blocking of the pores in the clinoptilolite zeolites, resulting in the decrease of surface areas and micropore volumes available in the modified zeolites (Table 3). According to Cañizares and Carrero (24), ferrierite with its H^+ ion exchanged with bulky cations of alkaline earth metals exhibited a similar tendency. In the case of clinoptilolite zeolites, however, more-pronounced changes were observed compared with that of ferrierite, probably due to the smaller pore size and the less available space in this zeolites (15).

NH_3-TPD was carried out over modified natural zeolites and ferrierite to measure the strength and amount of acid sites in these zeolites. As shown in Fig. 5, metal-cation-exchanged natural zeolites (Co–HNZ and Ba–HNZ) revealed different acid characteristics in terms of acid strength and amount compared with those of unmodified natural zeolite. The peak temperature reflects relative acid strength if possible shifts in the temperature of desorption due to readsorption of ammonia are comparable (25). All catalysts showed two NH_3 desorption peaks. The large first peak is due to weak acid sites, but the second peak, due to strong acid sites, is more relevant to skeletal isomerization reactions that require rather strong acid catalysts. Both the amount and the relative strength of acid sites for Co–HNZ and Ba–HNZ were decreased from those of HNZ. While Co–HNZ showed only a small shift in the second

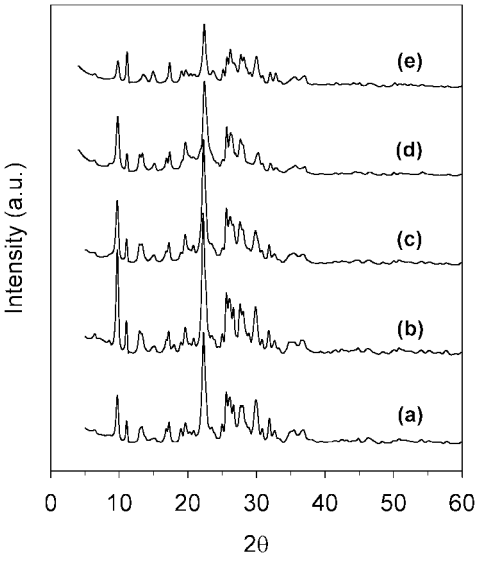

FIG. 4. XRD patterns of metal-cation-exchanged natural clinoptilolite zeolites. (a) Natural zeolite (NZ), (b) ammonium-form natural zeolite (NH^{4+}–NZ), (c) proton-form natural zeolite (HNZ), (d) Co–HNZ, (e) Ba–HNZ.

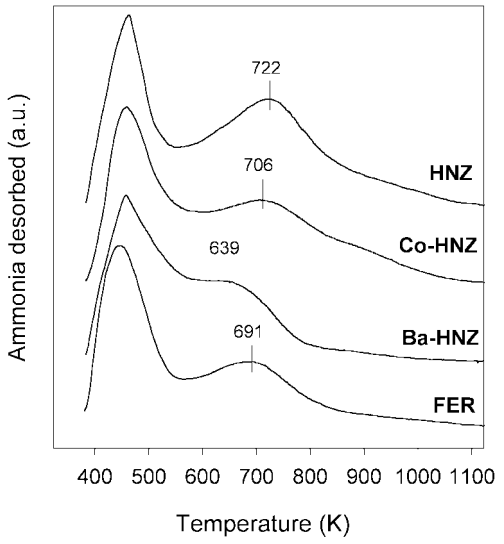

FIG. 5. NH_3-TPD profiles for HNZ, Co–HNZ, Ba–HNZ, and ferrierite.

desorption peak toward a lower temperature and preferential decrease in the peak area of only strong acid sites, Ba–HNZ showed a large shift of the strong acid site peak to a lower temperature as well as a drastic decrease in the area of both peaks.

The nature of acid sites was investigated by FT-IR studies of catalysts themselves and pyridine chemisorbed on them. Figure 6 shows the FT-IR spectra of the hydroxyl groups in the zeolites. The band at 3742 cm^{-1} is known to be due to the OH stretching of surface silanol group (Si–OH), and peaks at 3600–3630 cm^{-1} could be assigned as acidic hydroxyl groups from the bridging OH of Si–OH–Al, that is, Brønsted acid sites. From the wavenumbers of the acidic hydroxyl groups of HNZ (3600 cm^{-1}), Co–HNZ (3630 cm^{-1}), and Ba–HNZ (3610 cm^{-1}), we can consider that the relative strength of the Brønsted acid sites is HNZ > Ba–HNZ > Co–HNZ. Infrared spectrum of Ba–HNZ showed a narrower distribution of Brønsted acid sites compared with that of fresh zeolite, HNZ. The infrared spectrum of Co–HNZ revealed a new broad band at 3670 cm^{-1}, which could be assigned to an Al–OH group derived from the Si–OH–Al group or a Si–OH group shifted downfield due to the proton interaction (26).

FT-IR spectra of pyridine-chemisorbed zeolites are presented in Fig. 7. Although the small kinetic diameter of NH_3 (~2.6 Å) allows its access to all the acid sites in pores of

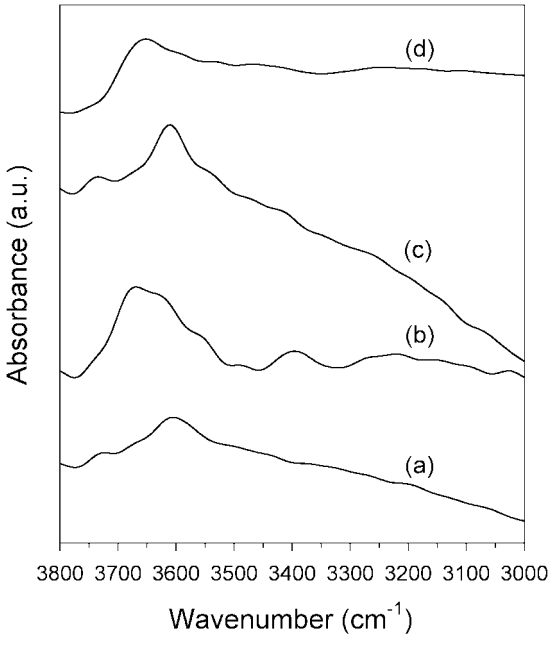

FIG. 6. FT-IR spectra in the hydroxyl group region of zeolites. (a) HNZ, (b) Co–HNZ, (c) Ba–HNZ, (d) ferrierite.

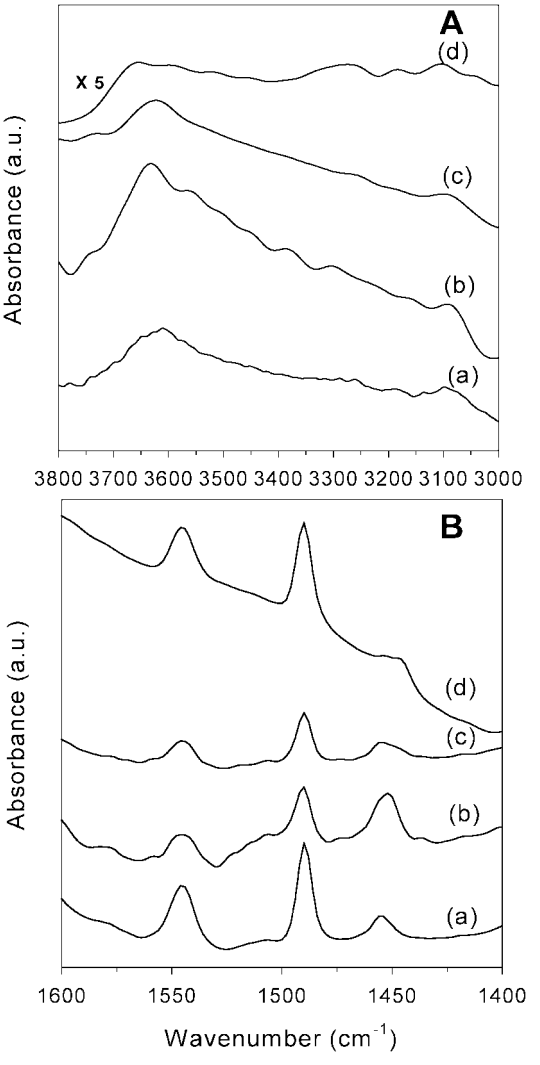

FIG. 7. FT-IR spectra of pyridine-chemisorbed zeolites: (A) In the region of hydroxyl group of zeolites; (B) in the region of adsorbed pyridine showing Brønsted and Lewis acid sites. (a) HNZ, (b) Co–HNZ, (c) Ba–HNZ, (d) ferrierite.

TABLE 4

Comparison of Acid Characteristics of HNZ, Ba–HNZ, Co–HNZ, and HFER

Catalysts	BET surface area (m^2/g)	NH_3–TPD: Peak temp (K)[a] T_L	T_H	Amount of desorbed NH_3 (μmol/g) T_L	T_H	Total amount of desorbed NH_3 (μmol/g)	Total acid sites, including B and L acid sites ($\mu mol/m^2$)	Pyridine FT–IR (L/B[b])
HNZ	219.3	459	722	667	1318	1985	9.05	0.48
Ba–HNZ	94.1	459	639	600	854	1454	15.45	1.03
Co–HNZ	161.8	459	706	660	1206	1866	11.53	4.65
HFER	210.7	448	691	544	726	1270	7.49	0.50

[a] T_L and T_H denote low and high desorption temperatures of ammonia, representing weak and strong acid sites, respectively.
[b] The ratio of peak areas representing L (Lewis acid site) at 1454 cm^{-1} and B (Brønsted acid site) at 1546 cm^{-1}.

microporous materials, pyridine may not approach the acid sites in relative small pores due to its larger kinetic diameter (~5.85 Å) (27). This is manifested by the fact that, as shown in Fig. 7A, HNZ and modified HNZs show the bands of an acidic hydroxyl group at 3600–3630 cm^{-1} even after chemisorption of pyridine. For Ba–HNZ, the peak intensity of an acidic hydroxyl group at 3610 cm^{-1} was decreased to a greater extent after pyridine chemisorption, due to a relatively large amount of exposed acid sites accessible by pyridine. Co–HNZ, however, still maintained the acidic hydroxyl group at 3630 cm^{-1}, as shown in Fig. 7A, spectrum b. Thus, a large portion of acid sites in Co–HNZ were not accessible by pyridine, mainly due to highly restricted inner space around the sites. In the case of ferrierite, most of acidic hydroxyl groups disappeared, indicating that pyridine can approach nearly all Brønsted acid sites in the pores of ferrierite under the condition of pyridine chemisorption experiments, as was discussed in Refs. (28, 29). The new bands at 3400–3000 cm^{-1} in Fig. 7A derived from the ring and C–H stretching of adsorbed pyridine. As shown in Fig. 7B, the number of Brønsted acid sites represented by the band at 1546 cm^{-1} decreased upon ion exchange of HNZ with Co or Ba. Instead, the intensity of the band at 1454 cm^{-1}, due to Lewis acid sites, increased for the modified zeolites. The number of Brønsted acid sites was in the order HNZ > Ba–HNZ > Co–HNZ and the order of the number of Lewis acid sites was the opposite. The acid characteristics of HNZ, metal-ion-exchanged HNZs, and ferrierite determined from ammonia TPD and FT-IR are summarized in Table 4. A parameter that stands out most for the selective Co–HNZ catalyst was the high ratio of Lewis acid sites to Brønsted acid sites (L/B) measured by FT-IR peak areas at 1454 cm^{-1} and 1546 cm^{-1}, respectively. It is known that Lewis acid sites have no important role in activity and selectivity for the skeletal isomerization of 1-butene. However, the high L/B ratio observed for Co–HNZ upon ion exchange of proton with Co indicates the decreased aerial concentration of Brønsted acid sites.

The structural change induced by metal cation exchange in the natural clinoptilolite zeolite was investigated through solid-state NMR experiments. ^{27}Al MAS NMR spectra of modified zeolites, shown in Fig. 8A, revealed two resolved

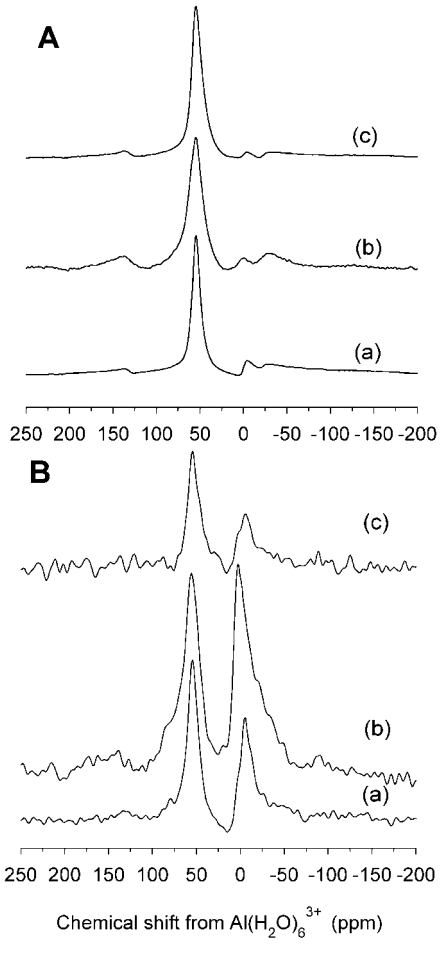

FIG. 8. Solid-state ^{27}Al NMR spectra of zeolites. (A) ^{27}Al MAS NMR (magic-angle spinning) spectra; (B) 27Al CP MAS NMR (cross-polarization magic-angle spinning) spectra. (a) HNZ, (b) Co–HNZ, (c) Ba–HNZ.

peaks, at 54 and –3 ppm, indicating nonequivalent magnetic Al centers present in the sample. These peaks can be assigned as tetrahedral and octahedral Al centers coordinated with donor atoms, respectively. As can be seen in Fig. 8A, ^{27}Al MAS NMR results for HNZ show a strong narrow resonance line of four-coordinated Al sites, but a low intensity of six-coordinated Al sites. Only considering four coordination in NMR spectra, we could obtain a NMR spectrum for Co–HNZ broader than that for HNZ. The broadened spectrum of Co–HNZ in Fig. 8A (spectrum b) indicates the presence of interaction between resonant nucleus and Co, where the metal cation, Co, might be considered a paramagnetic impurity. It is interesting that the ^{27}Al CPMAS NMR spectrum of Co–HNZ in Fig. 8B (spectrum b) exhibits a greatly enhanced intensity of six-coordinated aluminum center at –3 ppm due to the cross-polarization effect. That is, magnetization transfer from proton to aluminum centers occurred more easily at the six-coordinated than the four-coordinated Al center. This ^{27}Al CPMAS NMR result strongly suggests that six-coordinated Al is considered to be composed of extraframework zeolite channels in the form of Al–OH groups. ^{29}Si MAS NMR spectra of the modified zeolites are shown in Fig. 9. The spectra were deconvoluted into three peaks: peak 1, at –110 ppm, represents silicon with no aluminum neighbor, Si(0Al); and peaks 2 and 3, at –105 and –97 to –99 ppm, correspond to silicon with one aluminum, Si(1Al), and two aluminums, Si(2Al), respectively. Table 5 presents parameters obtained from ^{29}Si MAS NMR spectra such as linewidths and integrals (percentage) of deconvoluted Si(nAl) peaks. The deconvoluted ^{29}Si MAS NMR spectrum of Co–HNZ exhibited higher intensity for the Si(0Al) peak and greater linewidth than those of other zeolites. This result of NMR could be understood by the formation of a terminal silanol group (Si–OH) upon ion exchange of natural clinoptilolite zeolite with cobalt ion. This is also supported by the substantial increase in the intensity of the Si–OH IR band in Fig. 6b. The formation of extraframework Al–OH and Si–OH groups indicate substantial modification of the external surface and space around the pores.

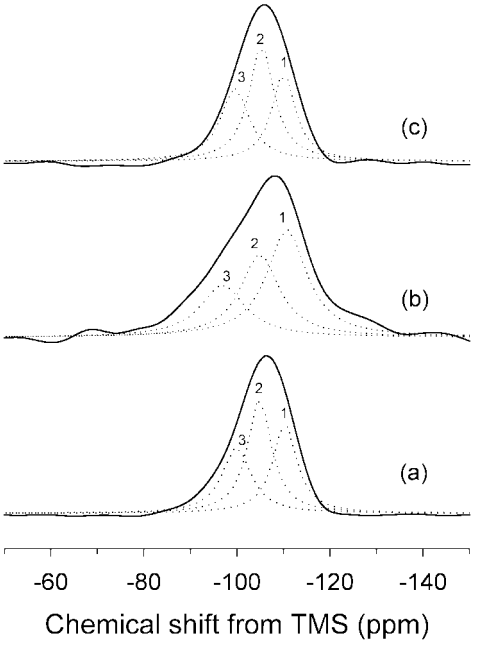

FIG. 9. Solid-state ^{29}Si MAS NMR spectra of zeolites. (a) HNZ, (b) Co–HNZ, (c) Ba–HNZ.

TABLE 5

Analysis Results of ^{29}Si MAS NMR Spectra over Proton-Form Natural Zeolite (HNZ) and Metal-Ion-Exchanged Zeolites (Co–HNZ and Ba–HNZ)

Catalyst	Peak	Position (ppm)	Width (ppm)	Integral (%)
HNZ	1	−110.3	6.1	31.6
	2	−104.9	6.0	40.2
	3	−99.9	7.4	28.2
Co–HNZ	1	−110.7	10.0	43.6
	2	−105.0	10.3	32.6
	3	−96.9	11.7	23.9
Ba–HNZ	1	−110.1	6.0	29.3
	2	−105.3	6.4	41.1
	3	−99.6	7.3	29.6

DISCUSSION

The controlling factors for the selectivity of isobutene in the skeletal isomerization of 1-butene were investigated in this study through comparison of zeolite pore structure and acid characteristics. There are many factors affecting the selectivity of isobutene in skeletal isomerization of 1-butene and they have been discussed by many researchers (10–14). Among the factors, the characteristics of pore structure in various zeolites and molecular sieves are most likely to affect the selectivity of isobutene by shape selectivity, and their effects are usually investigated by employing zeolites with different structures. When the zeolite structure is fixed, other factors, including acidity in particular, are also important. The role of acidity in the skeletal isomerization of 1-butene could be considered in several aspects, such as type, density, strength, and accessibility of acid sites.

In this study, we compared the catalytic performance of ferrierite, natural clinoptilolite zeolite, and clinoptilolite zeolites modified with metal cations for the skeletal isomerization of 1-butene. While all the clinoptilolite zeolites exhibited higher selectivity than that of ferrierite, conversion of *n*-butenes for ferrierite was much higher under the same reaction conditions, as shown in Table 2. Thus, this difference could be partly attributable to the higher conversions over ferrierite. However, the intrinsically higher isomerization selectivity for clinoptilolite zeolite compared

with that of ferrierite was established by Seo *et al.* (23) at a nearly equivalent level of conversion. From the simulated distributions of 1-butene molecules on clinoptilolite and ferrierite zeolites, they noted the difference in the degree of restriction on adsorption of 1-butene on acid sites in the zeolite pores. Thus, more-favorable diffusion of the reactant is possible into the relatively wide pores (4.2×5.4 Å in 10-membered rings) of ferrierite compared with the narrower pores (7.5×3.1 Å in 10-membered rings) of clinoptilolite zeolite, which are more elliptically shaped. On the other hand, the more restricted pore structure of clinoptilolite resulted in higher selectivity of isobutene by suppressing the major side reaction of dimerization followed by cracking, which is favored in more spacious pores (10).

Modification of proton-form natural clinoptilolite zeolite (HNZ) with various metal cations resulted in different acid properties in terms of type, density, strength, and accessibility of the acid sites. Although decrease in surface areas and micropore volumes was observed in metal-cation-exchanged HNZs, these modified zeolites (Me–HNZs) maintained the clinoptilolite framework, as revealed in Fig. 4.

Among metal-cation-exchanged zeolites, Co–HNZ was unique in exhibiting higher selectivity of isobutene without much change in the conversion of *n*-butenes, compared with that of HNZ. Various characterization techniques, such as NH_3-TPD, FT-IR, and solid-state NMR experiments, allowed us to identify acid characteristics of Co–HNZ when the results obtained from different techniques were considered together. The higher selectivity of isobutene for Co–HNZ could be attributed to the preferential decrease in the number of strong acid sites together with a small decrease in acid strength, as determined from NH_3-TPD (in Fig. 5), and also to the high ratio of Lewis acid sites relative to Brønsted acid sites (L/B), determined from FT-IR spectroscopy of chemisorbed pyridine (in Fig. 7B, spectrum b). The last property would reduce the concentration of Brønsted acid sites. It has been shown that high concentrations of Brønsted acid sites reduce the isobutene selectivity by increasing the chance of consecutive reactions of primary products to produce by-products (11). Moreover, an enhanced constraint on the accessibility to acid sites residing in the pores of Co–HNZ could be ascertained by observing the remaining hydroxyl groups after pyridine chemisorption (in Fig. 7A, spectrum b). The modification might be accompanied by forming Al–OH and Si–OH groups consisting of extraframework zeolite, as shown by FT-IR in Fig. 6b, by ^{27}Al CP MAS NMR (in Fig. 8B, spectrum b), and ^{29}Si MAS NMR of Co–HNZ (in Fig. 9b). In this respect, the results of FT-IR and NMR exhibited a good correspondence for cobalt-ion-exchanged clinoptilolite zeolite.

Thus, ion exchange of natural clinoptilolite zeolite (HNZ) with cobalt cation gives rise to a proper control of acid properties as well as an effective steric constraint of the clinoptilolite pore structure, leading to a more selective reaction pathway.

Ba–HNZ revealed a greatly reduced surface area and relatively poor crystallinity, which might be due to the partial collapse of framework and pore blocking induced by ion exchange and subsequent steps, as shown in Table 3. It showed, however, a highly increased conversion of *n*-butenes but low selectivity of isobutene, yielding a large amount of by-products ($C_3 + C_5$), as exhibited in Table 2. From the catalytic performance of Ba–HNZ, we could consider the possibility of a bimolecular mechanism that forms not only desired isobutene but also by-products through a subsequent cracking reaction. Čejka *et al.* (30) reported that at least 30% isobutene was produced over ferrierite and 6% over CoAlPO-11 through a bimolecular mechanism, which was investigated using ^{13}C-labeled 1-butene. It was concluded that a high selectivity of isobutene could be obtained only via a monomolecular pathway. In any case, the bimolecular mechanism yielding isobutene seems to operate in Ba–HNZ to a higher extent than in HNZ and Co–HNZ.

Ba–HNZ revealed a narrow distribution of an acidic bridging hydroxyl group, Brønsted acid sites (Fig. 6c), though the amount and strength of acid sites were greatly decreased from those of HNZ, as shown in NH_3-TPD (Fig. 5). Furthermore, Ba–HNZ has more accessible acid sites, as evidenced by a greatly reduced amount of Brønsted acid sites upon pyridine adsorption, as shown in Fig. 7A (spectrum c). Furthermore, the total number of acid sites including Brønsted and Lewis acid sites per surface area was 15.45 μmol/m^2 for Ba–HNZ compared with 9.05 μmol/m^2 for HNZ, as shown in Table 4. After taking these results and considerations about Ba–HNZ (low surface area, partially collapsed pore structure, some pore blocking, increased extent in the bimolecular mechanism, lower amount and high accessibility to acid sites) into consideration, we reached the conclusion that a large part of the skeletal isomerization of 1-butene on Ba–HNZ would proceed at the acid sites on the external surface. These acid sites, however, could be considered nonselective reaction sites, leading to an increase in the extent of the bimolecular reaction pathway.

In summary, it can be suggested that the high density and easy accessibility of acid sites in Ba–HNZ may have resulted in the increased extent of the bimolecular reaction pathway. These appears to be attributes of ferrierite as well, showing a high reaction rate but a low isobutene selectivity. On the other hand, higher selectivity over the Co–HNZ catalyst could be induced by selective elimination of strong acid sites that are responsible for side reactions such as dimerization and cracking as well as by an effective steric constraint on zeolite channels that would reduce the possibility of bimolecular reactions. Thus, important factors for a selective catalyst in the skeletal isomerization are related to the acid characteristics, such as proper acid strength, low

concentration of the acid sites, and a high ratio of Lewis acid sites to Brønsted acid sites (L/B), as well as to a unique pore structure that imposes effective steric constraints on the possible bimolecular reaction.

CONCLUSIONS

Cobalt-cation-exchanged natural clinoptilolite zeolite showed higher selectivity to isobutene in the skeletal isomerization of 1-butene compared with that of proton-form natural clinoptilolite at the same conversion of *n*-butenes under the same reaction conditions. The high selectivity for cobalt-exchanged zeolite was mainly attributed to the selective elimination of strong acid sites that could give rise to the undesired side reactions. As a result, a high ratio of Lewis acid sites to Brønsted acid sites (L/B) was observed in selective cobalt-ion-exchanged zeolite. Barium-cation-exchanged zeolite exhibited a higher activity but a very low selectivity to isobutene. The high density and easy accessibility of acid sites for barium-ion-exchanged zeolite seemed to increase the extent of the bimolecular reaction pathway, leading to a high yield of by-products. Thus, a selective catalyst for skeletal isomerization of 1-butene should satisfy multiple requirements regarding its acid site, namely, strength, type, concentration, and accessibility.

ACKNOWLEDGMENTS

The authors acknowledge the financial support of the Korea Research Foundation made in the program year 1998. This work was also supported by the BK 21 program of the Korea Ministry of Education & Human Resources Development.

REFERENCES

1. Hutchings, G. J., Nicolaides, C. P., and Scurrel, M. S., *Catal. Today* **15**, 23 (1992).
2. Butler, A. C., and Nicolaides, C. P., *Catal. Today* **18**, 443 (1993).
3. Houžvička, J., and Ponec, V., *Catal. Rev.–Sci. Eng.* **39**(4), 319 (1997).
4. Mooiweer, H. H., de Jong, K. P., Kraushaar-Czarnetzki, B., Stork, B. W. H., and Krutzen, B. C. H., *Stud. Surf. Sci. Catal.* **84**, 2327 (1994).
5. Pellet, R. J., Casey, D. G., Huang, H.-M., Kessler, R. V., Kuhlman, E. J., O'Young, C.-L., Sawicki, R. A., and Ugolini, J. R., *J. Catal.* **157**, 423 (1995).
6. Xu, W.-Q., Yin, Y.-G., Suib, S. L., Edwards, J. C., and O'Young, C.-L., *J. Catal.* **163**, 232 (1996).
7. Simon, M. W., Suib, S. L., and O'Young, C.-L., *J. Catal.* **147**, 484 (1994).
8. Xu, W.-Q., Yin, Y.-G., Suib, S. L., and O'Young, C.-L., *J. Catal.* **150**, 34 (1994).
9. Gielgen, L. H., Veensta, I. H. E., Ponec, V., Haanepen, M. J., and Van Hooff, J. H. C., *Catal. Lett.* **32**, 195 (1995).
10. O'Young, C.-L., Pellet, R. J., Casey, D. G., Ugolini, J. R., and Sawicki, R. A., *J. Catal.* **151**, 467 (1995).
11. Houžvička, J., Hansildaar, S., and Ponec, V., *J. Catal.* **167**, 273 (1997).
12. Mériaudeau, P., Tuan, V. A., Hung, L. N., Naccache, C., and Szabo, G., *J. Catal.* **171**, 329 (1997).
13. Seo, G., Jeong, H. S., Lee, J. M., and Ahn, B. J., *Stud. Surf. Sci. Catal.* **105**, 1431 (1997).
14. Seo, G., Kim, N.-H., Lee, Y.-H., and Kim, J.-H., *Catal. Lett.* **51**, 101 (1998).
15. Szostak, R., "Handbook of Molecular Sieves." Van Nostrand Reinhold, New York, 1992.
16. Tihmillioglu, F., and Ulku, S., *Sep. Sci. Tech.* **31**, 2855 (1996).
17. Arcoya, A. X., Seoane, L., and Soria, J., *J. Chem. Tech. Biotechnol.* **68**, 171 (1997).
18. Allahverdiev, A. I., Irandoust, S., and Murzin, D. Y., *J. Catal.* **185**, 352 (1999).
19. Linares, C. F., Goldwasser, M. R., Machado, F. J., Rivera, A., Rodríguez-Fuentes, G., and Barrault, J., *Microporous Mesoporous Mater.* **41**, 69 (2000).
20. Woo, H. C., Lee, K. H., and Lee, J. S., *Appl. Catal. A* **134**, 147 (1996).
21. Lee, H. C., Woo, H. C., Ryoo, R., Lee, K. H., and Lee, J. S., *Appl. Catal. A* **196**, 135 (2000).
22. Morris, R. E., Weigel, S. J., Henson, N. J., Bull, L. M., Janicke, M. T., Chmelka, B. F., and Cheetham, A. K., *J. Am. Chem. Soc.* **116**, 11849 (1994).
23. Seo, G., Kim, M.-W., Kim, J.-H., Ahn, B. J., Hong, S. B., and Uh, Y. S., *Catal. Lett.* **55**, 105 (1998).
24. Cañizares, P., and Carrero, A., *Catal. Lett.* **64**, 239 (2000).
25. Katada, N., Igi, H., Kim, J. H., and Niwa, M., *J. Phys. Chem. B* **101**, 5969 (1997).
26. Macche, M., Janin, A., and Lavalley, J. C., *Zeolites* **13**, 419 (1993).
27. Lee, Y.-K., Park, S.-H., and Rhee, H.-K., *Catal. Today* **44**, 223 (1998).
28. Pieterse, J. A. Z., Veefkind-Reyes, S., Seshan, K., Domokos, L., and Lercher, J. A., *J. Catal.* **187**, 518 (1999).
29. Trombetta, M., and Busca, G., *J. Catal.* **187**, 521 (1999).
30. Čejka, J., Wichterlová, B., and Sarv, P., *Appl. Catal. A* **179**, 217 (1999).